Large Current Modulation and Spin-Dependent Tunneling of Vertical Graphene/MoS_2 Heterostructures

Nojoon Myoung,[†] Kyungchul Seo,[†,§] Seung Joo Lee,[‡,*] and G. Ihm[†,*]

[†]Department of Physics, Chungnam National University, Daejoen 305-764, Republic of Korea and [‡]Quantum-functional Semiconductor Research Center, Dongguk University, Seoul 100-715, Republic of Korea. [§]Present address: Daeduk Campus for BNT Convergence, Paichai University, Daejeon 305-509, Republic of Korea.

ABSTRACT Vertical graphene heterostructures have been introduced as an alternative architecture for electronic devices by using quantum tunneling. Here, we present that the current on/off ratio of vertical graphene field-effect transistors is enhanced by using an armchair graphene nanoribbon as an electrode. Moreover, we report spin-dependent tunneling current of the graphene/MoS_2 heterostructures. When an atomically thin MoS_2 layer sandwiched between graphene electrodes becomes magnetic, Dirac fermions with different spins feel different heights of the tunnel barrier, leading to spin-dependent tunneling. Our finding will develop the present graphene heterostructures for electronic devices by improving the device performance and by adding the possibility of spintronics based on graphene.

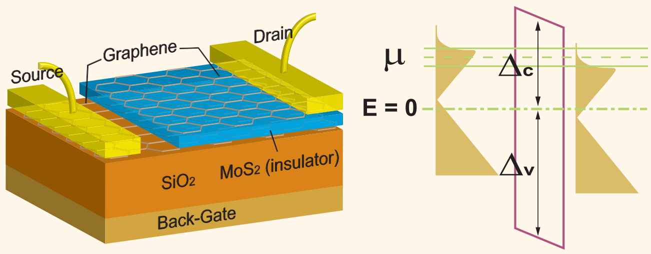

KEYWORDS: quantum tunneling · graphene · MoS_2 · vertical heterostructure · field-effect transistor · spin filter

Graphene has been considered to be a promising material for future electronics due to its extraordinary properties such as high carrier mobility,[1,2] thermal conductivity,[3] and strong break strength.[4] Although the extremely high electrical conductivity makes graphene a potential candidate for replacing silicon-based electronics, Klein tunneling causes the electrical transport of Dirac fermions to be insensitive to electrostatic potentials, resulting in a low current on/off ratio of graphene-based field-effect transistors.[5−7] In order to realize graphene electronics, it is important to manipulate its electronic properties without impairing its high mobility.

Recently, increasing interest has been focused on an alternative graphene device structure by using quantum tunneling. For a graphene/silicon heterojunction, a large current on/off ratio was achieved by controlling the Schottky barrier formed at the interfaces.[8] In spite of the device performance, the carrier mobility of graphene deposited on a silicon substrate is generally expected to decrease because of the inhomogeneity caused by the substrate.[9,10] Meanwhile, the possibility of a graphene field-effect transistor has been reported, based on vertical heterostructures with atomically thin insulating barriers such as hexagonal boron nitride (hBN) and molybdenum disulfide (MoS_2).[11−14] Layered materials such as hBN and MoS_2 have gained burgeoning interest as a material for use in graphene devices.[15] For example, the encapsulation of graphene by hBN maintains the high electronic quality of pristine graphene.[16−19] While the large band gap of hBN (~5.97 eV[20]) causes an insufficient current on/off ratio, a larger on/off ratio was observed for a graphene/MoS_2 vertical field-effect transistor, owing to its smaller band gap as compared to hBN. Therefore, the graphene/MoS_2 heterostructure has been regarded as a significant building block of graphene-based electronics, and it is important to investigate possible functional devices by utilizing its advantages for applications.

Herein, we present not only the improvement in the current on/off ratio of the existing graphene/MoS_2 vertical field-effect transistors[11] but also an application of the heterostructure in spintronics by producing spin-dependent tunneling. First, we show

* Address correspondence to ghihm@cnu.ac.kr; leesj@dongguk.edu.

Received for review May 2, 2013 and accepted July 23, 2013.

Published online July 23, 2013
10.1021/nn402919d

that there emerges a peak nature in the tunneling current characteristics for a graphene/MoS_2/graphene nanoribbon (GNR) heterostructure. This finding has potential for the use of current peaks, resulting in the improvement of the current on/off ratio. Second, the existence of magnetic properties in few-layer MoS_2[21−26] can lead to a spin-polarized current in graphene heterostructures. We show that the graphene heterostruture can be a perfect spin-filter for holes with the electron−hole asymmetric spin splitting of MoS_2.[27] Such tunneling phenomena may lead to further potential applications in graphene-based electronics and spintronics.

Now, we consider a heterostructure that consists of an atomically thin MoS_2 layer sandwiched between two graphene sheets as shown in Figure 1a. It is well known that few-layer MoS_2 is an insulator with finite band gaps: a ∼1.9 eV direct band gap near the K-valley and a ∼1.2−1.4 eV indirect band gap depending on the number of MoS_2 layers.[28−31] The MoS_2 layer of the heterostructure becomes a tunnel barrier for Dirac fermions, and both the graphene sheets play the role of high-quality source and drain electrodes. Dirac fermions experience the direct band gap near the K-valley of MoS_2 rather than the smallest indirect band gap because of the momentum conservation, neglecting electron−phonon scattering processes.

RESULTS AND DISCUSSION

The tunneling current through the MoS_2 insulating barrier can be obtained as below

$$j(V_b, V_g) = j_0 \int_{-\infty}^{+\infty} D_s(E, V_b)\, D_d(E, V_b)\, T(E)[f_s(E, V_b, V_g) - f_d(E, V_b, V_g)]\, dE \qquad (1)$$

where $j_0 = (qv_F)/(2\pi L_0^2)$ is the unit of current density with electric charge of carriers q and the characteristic length of the system L_0. The transmission probability $T(E)$ can be calculated quantum mechanically (see Supporting Information). Here, D_i and f_i are density of states of graphene and the Fermi−Dirac distribution, where i = s, d represent source and drain graphene electrodes on both sides of the MoS_2 layer, respectively.

By applying gate voltage V_g *via* a back gate electrode, carriers are induced on the top and bottom graphene layers. Simply, it can be assumed that the equal carrier concentration is induced on both graphene layers; $n = \alpha V_g$ where $\alpha = 6.16 \times 10^{14}\ \mathrm{Cs^2\,kg^{-1}\,m^{-4}}$ in the case of a 350 nm thick SiO_2 substrate. Under this assumption, the chemical potential on both graphene layers are equally given as $\mu = \hbar v_F(\pi|n|)^{1/2} = \hbar V_F(\pi\alpha|V_g|)^{1/2}$ for the given V_g. In the absence of the bias voltage V_b between the top and bottom graphene layers, no net tunneling current is produced. Applying V_b, one can measure a nonzero tunneling current through the heterostructures. However, in fact, the effects of the interlayer screening between the top and bottom graphene layers must be taken into account in order to perform a much more detailed analysis of practical device performance. Since the interlayer screening length of graphene is short enough (∼0.6 nm[32]), the bottom graphene layer, where carriers are induced by V_g, can affect the carrier concentration on the top graphene

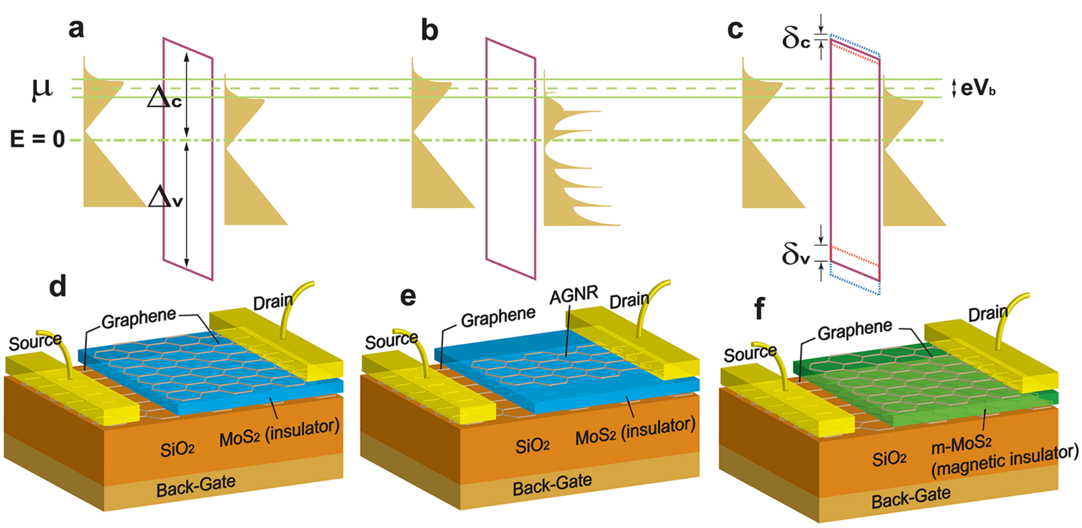

Figure 1. Schematics of various graphene/MoS_2 heterostructures considered in this study. (a−c) Energetic diagrams for quantum tunneling through MoS_2 insulating barriers for various heterostructures: graphene/MoS_2/graphene, graphene/MoS_2/AGNR, and graphene/m-MoS_2/graphene, respectively. The chemical potential μ is formed by back gate voltage V_g, and the tunneling current is generated by bias voltage V_g applied between the source and drain graphene electrodes. Since the charge neutral point of graphene is asymmetrically laid, electrons and holes experience different tunnel barriers, Δ_c and Δ_v. (b) If one graphene electrode is replaced by a narrow GNR, the density of states is changed, reflecting the one-dimensional nature. (c) When the MoS_2 layer becomes magnetic, the barrier height is spin-dependent with different spin-splitting energies, δ_c and δ_v. (d−f) Schematic diagrams of various heterostructures corresponding to (a), (b), and (c), respectively.

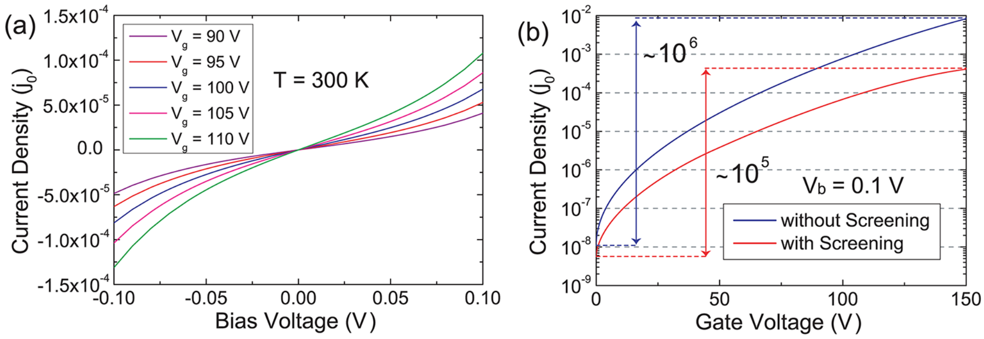

Figure 2. Tunneling current characteristics of a graphene/MoS_2/graphene heterostructure. (a) Tunneling current density through a graphene/MoS_2/graphene heterostructure as a function of bias voltage for different gate voltages at 300 K. (b) Tunneling current *versus* gate voltage for the given bias voltage with and without the interlayer screening between two graphene layers. The calculated tunneling current density is normalized by the current unit $j_0 = (qv_F)/(2\pi L_0^2)$.

layer. For the given V_g, the carrier concentration induced on both graphene layers is calculated by solving Poisson's equation with inhomogeneous media (see Supporting Information). As a consequence of the screening by the bottom layer, always fewer carriers are induced in the top layer compared to the bottom layer. Due to this difference, the Dirac cone of the top graphene layer shifts in order to bring the system into equilibrium.

Figure 2 displays the characteristics of the graphene/MoS_2/graphene field-effect transistor. The calculated tunneling currents as a function of V_b for different V_g are shown in Figure 2(a). The tunneling current exhibits the increasing behavior with V_b and becomes larger as V_g increases. Here, note the fact that the tunneling current density is asymmetric with respect to bias voltage. This asymmetric feature of the tunneling current is a consequence of the interlayer screening. Even at equilibrium (V_b = 0 V), there exists a finite electric field between the top and bottom graphene layers, which induces the shift of the Dirac cone. When V_b is applied between the two graphene layers, the number of carriers, which contribute to tunneling, is differently induced, depending upon the direction of V_b.

The tunneling current curve *versus* V_g is plotted in Figure 2(b). The ratio of the tunneling current density between an off-state (V_g = 0 V) and an on-state (V_g = 150 V) is found for the given V_b at room temperature. While the current on/off ratio without the screening effect reaches up to 10^6, it goes down to 10^5 in consideration of the screening effect. Despite this decrease, the room-temperature current on/off ratio is still as high as experimentally reported in ref 11.

For graphene/MoS_2 hybrid systems, the charge neutral point of the Dirac cone is asymmetrically arranged between the conduction and valence bands near the K-valley of MoS_2.[33] Thus, electrons experience a smaller tunnel barrier ($\Delta_c \approx 0.5$ eV) than holes ($\Delta_v \approx 1.4$ eV), where Δ_c and Δ_v are the barrier heights for electrons and holes, respectively. Therefore, if the tunneling electrons and holes are at the same chemical potential, the transmission probability through the MoS_2 insulating barrier for electrons is greater than for holes. Figure 3(a) exhibits the difference in tunneling current for electrons and holes as a function of V_g. We find that the tunneling current is indeed asymmetric with respect to the gate voltage polarity. The asymmetry also appears in the current on/off ratio as shown in Figure 3(b). This result implies that it is advantageous to use electron tunneling for the vertical graphene/MoS_2 field-effect transistor. At this moment, let us note that the carrier-dependent tunneling current can

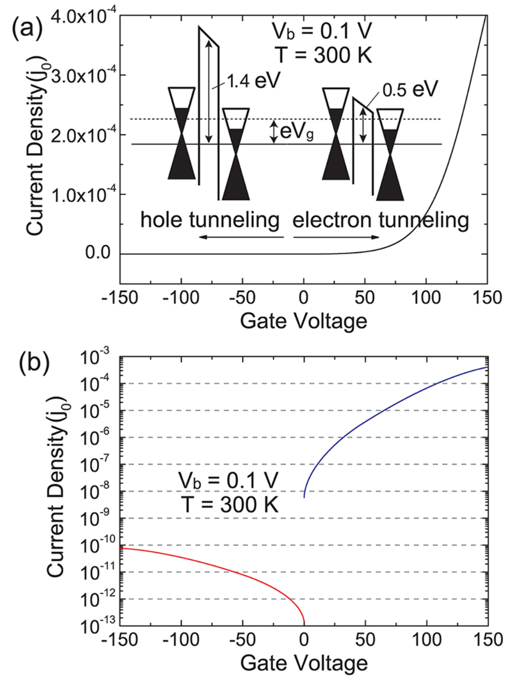

Figure 3. Electron–hole asymmetry of tunneling current of a graphene/MoS_2/graphene heterostructure. (a) Asymmetric tunneling current density curve *versus* gate voltage at 300 K for V_b = 0.1 V. Inset: Energetic diagrams for electron and hole tunneling. Electrons and holes experience different heights of tunnel barriers because of the asymmetric arrangement of the Dirac cone for the graphene/MoS_2 hybrid system. (b) Linear-log plot of the electron and hole tunneling current density as a function of gate voltage. The current on/off ratio is also asymmetric for different kinds of carriers, electrons, and holes.

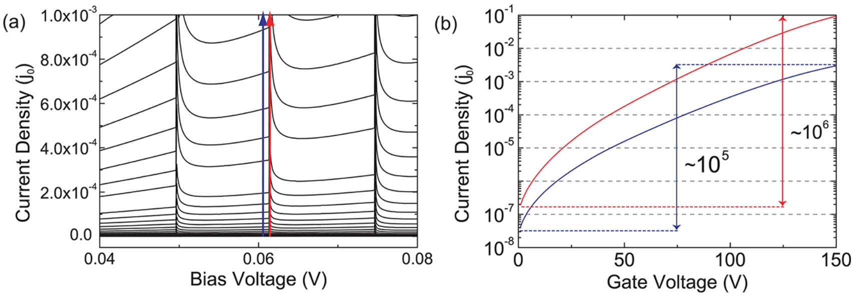

Figure 4. Enhancement of current on/off ratio of a graphene/MoS_2/AGNR heterostructure. (a) Tunneling current density through graphene/MoS_2/AGNR heterostructures at 300 K as a function of bias voltage for different gate voltages. Peaks emerge in current density curves at specific V_b due to the one-dimensional nature of AGNRs. (b) Comparison of the current on/off ratios in different cases: at peak (red lines) and near peak (blue lines), corresponding to panel a. The calculated tunneling density is normalized by $j_0 = (qv_F)/(2\pi L_0^2)$.

become controllable by doping MoS_2 layers (see Supporting Information).

Next, the current on/off ratio of the graphene/MoS_2/graphene field-effect transistor can be enhanced by considering finite size effects of a graphene electrode. A graphene electrode on one side of the sandwiched MoS_2 layer is replaced by a GNR, as shown in Figure 1(b). Since the tunneling current density depends on the product of density of states of source and drain electrodes (eq 1), one can expect changes in the tunneling current characteristics. In this paper, armchair graphene nanoribbons (AGNRs) are considered, of which the density of states exhibits a one-dimensional nature (see the Supporting Information). Here, note that we can choose either armchair or zigzag graphene nanoribbons because the improvement in the current on/off ratio originates from the one-dimensional nature (van Hove singularity) of the GNRs.

The resulting tunneling current through a graphene/MoS2/AGNR heterostructure is plotted in Figure 4(a) as a function of V_b for different V_g, at 300 K. Peaks emerge in the tunneling current density curves at specific V_b due to the existence of the van Hove singularities of the AGNR. This feature plays a crucial role in the enhancement of the current on/off ratio. Figure 4(b) shows linear-log plots of the tunneling current density as a function of V_g for different V_b, at 300 K. The magnitude of the current density for $V_b = V_{peak}$ (at a current peak, $V_{peak} \approx 0.06135$ V, blue lines) is 10 times larger than the background values (for $V_b = 0.061$ V, red lines). Due to the existence of the current peak, an abrupt change in the tunneling current by 1 order of magnitude emerges, and the resulting current on/off ratio is enhanced up to 10^6 if one adjusts V_b near V_{peak}. Therefore, the use of an AGNR instead of a two-dimensional graphene sheet as an electrode is attractive for applications in graphene-based electronics, improving the performance of the vertical graphene field-effect transistor.

In recent years, it has been found that the exhibited magnetic properties in an atomically thin MoS_2 layer can be due to several causes: zigzag-terminated grain boundary[21−24] or sulfur-vacancy.[25] For example, the broken inversion symmetry due to the sulfur-vacancy leads to a splitting between different spin states for few-layer MoS_2, whereas there is no spin-splitting for bulk MoS_2.[27] In this paper, we consider that the MoS_2 layer used in our heterostructure is thin enough to have a nonzero spin-splitting energy when inversion symmetry is broken. In this case, the thin MoS_2 layer can be treated as a magnetic insulator with a spin-dependent barrier height, $U(z) = \Delta_{c,v} + \sigma\delta_{c,v} + qV_b z/d$, where $\sigma = \pm 1$ represents different spins and $\delta_{c,v}$ indicates spin-splitting energies in the conduction and valence bands of MoS_2, respectively. Let us focus on the spin-splitting near the K-valley of MoS_2 because tunneling Dirac fermions experience the direct band gap near the K-valley rather than the indirect gap as aforementioned.

The calculation results of spin-dependent tunneling current through a magnetic MoS_2 (m-MoS_2) are shown in Figure 5. Here, the spin-polarization of the tunneling current density is defined as $P_j = (j_{up} - j_{down})/(j_{up} + j_{down})$. In Figure 5, one can see the differences in the spin-dependent feature for electron and hole tunneling currents. While the hole tunneling current is almost perfectly spin-polarized, the electron tunneling current is weakly spin-polarized. This is due to the fact that the spin-splitting near the K-valley of m-MoS_2 is about 50 times larger in the valence band ($\delta_v \approx 145$ meV) than in the conduction band ($\delta_c \approx 3$ meV).[27] The small spin-splitting energy in the conduction band leads to the relatively weak spin-polarization of the electron tunneling current, $P_j \approx 0.03-0.05$. Meanwhile, due to the large spin-splitting in the valence band, the hole tunneling current is almost perfectly spin-polarized, $P_j \approx 0.9-0.97$. The spin-dependence of the tunneling current is also asymmetric with respect to the bias voltage polarity as a consequence of the interlayer screening as aforementioned. Here, one may think that the large spin-polarization of the hole tunneling current seems to be unimportant because the hole tunneling is suppressed by the high tunnel barrier. This is resolved by using p-doped MoS_2 layers instead of intrinsic MoS_2. The hole tunneling current can be

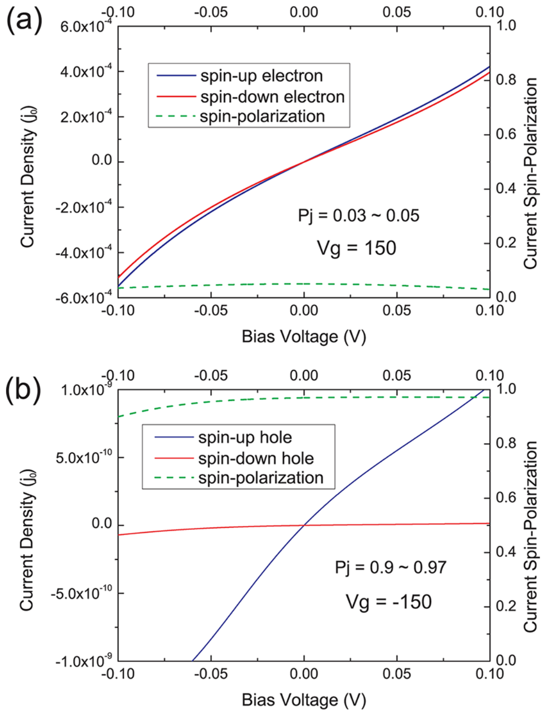

Figure 5. Spin-polarization of tunneling current near the K-valley. Spin-dependent current density through a graphene/m-MoS_2/graphene heterostructure for (a) electron and (b) hole tunneling. Blue and red solid lines indicate tunneling current densities for spin-up and -down carriers, respectively. Green dashed lines represent the spin-polarization of the tunneling current density.

increased by p-doping of MoS_2 layers as a consequence of reduction in the tunnel barrier height for holes (see the Supporting Information).

However, we need to consider the fact that there are two equivalent valleys in MoS_2 (K and K′) with opposite spin-splitting energies. (These equivalent valleys in MoS_2 are significant because the opposite Berry curvatures at these valleys may affect the transport properties of MoS_2 such as the cancellation of in-plane current.[34]) As a consequence, there should be the same amount of spin-up and spin-down Dirac fermions after tunneling through the spin-dependent tunnel barrier, and net current is non-spin-polarized in spite of the large spin-polarization near each valley. Here, let us introduce a strategy to achieve spin-polarized current in the graphene/m-MoS_2/graphene heterostructures: the valley-polarization in the graphene electrode. Since most of the spin-up (down) Dirac fermions in the drain graphene electrode are near the K (K′)-valley, we can achieve spin-polarized current if valley-polarization is generated by a valley-filter. It is well known that the trigonal warping breaks the valley symmetry in graphene at several 100 meV, and it has been revealed that the valley-polarization can be obtained through a p−n junction as a valley-filter[35,36] (see Supporting Information). In our systems, chemical potential in the top graphene electrode is ∼300 meV for V_g = 100 V, which is valid for the trigonal warping. We, therefore, expect that the spin-polarized current can be achieved by adding a valley-filter to our heterostructure. In the results, the graphene/m-MoS_2/graphene heterostructures provide a potential application in graphene-based spintronics as a good spin-filter, compared with the existing spintronics technology.[37]

CONCLUSIONS

In summary, we have investigated the characteristics of the tunneling current through graphene/MoS_2 heterostructures. We have done calculations for various heterostructures: graphene/MoS_2/graphene, graphene/MoS_2/AGNR, and graphene/m-MoS_2/graphene. It is shown that the current on/off ratio of the vertical graphene field-effect transistor based on a graphene/MoS_2/graphene heterostructure is up to 10^5 at room temperature. We have also found out that the vertical graphene field-effect transistor exhibits a carrier-dependent tunneling feature, which allows electrons to tunnel through the insulating barrier, more easily than holes. Furthermore, we have shown that the current on/off ratio of the vertical graphene field-effect transistor can be enhanced up to 10^6 by replacing a two-dimensional graphene electrode with an AGNR electrode. Using a ZGNR electrode also leads to the enhancement of the current on/off ratio because the enhancement originates from the van Hove singularity of GNRs. Finally, we propose a novel utility, the spin-polarized tunneling current, in the case where there exists a splitting between different spin states in the atomically thin MoS_2 layer. The different spin-splitting energy between the conduction and valence bands of MoS_2 makes the hole tunneling current almost perfectly spin-polarized, whereas the electron tunneling current is partially spin-polarized. Although the hole tunneling is small due to the carrier-dependent tunneling, it may be resolved by further studies on the effects of p-doping of MoS_2 layers. The graphene/m-MoS_2/graphene heterostructure may act as a spin-filter for holes, which can be a crucial building block of future spintronic devices. Our findings not only offer an advance in research on vertically stacked graphene heterostructures with thin insulating layers but also contribute to graphene-based electronics and spintronics.

METHODS

Computational Details. All tunneling current density data presented in this study were calculated numerically by using the Fortran computer program (Compaq Visual Fortran, version 6.6, Compaq Computer Corp.). The Fortran 90 codes to perform the numerical calculations were developed by implementing our own custom computational algorithm and subroutines from the IMSL package. The calculation of the transmission probabilities through insulating barriers, which is necessary to obtain the tunneling current density, was done in the direct tunneling regime. The curves of the nonlinear carrier concentrations from the self-consistent Poisson equation were performed in Mathematica (version 8.00, Wolfram Research, Inc.). The self-consistent problem was effectively solved by considering boundary conditions in static electrodynamics. For the graphene/MoS_2/AGNR heterostructures, the density of states of AGNR is given as an analytic formula since AGNR exhibits exact solutions for its eigenmodes, but plots of the density of states shown in the Supporting Information were obtained numerically by using Mathematica (version 8.00, Wolfram Research, Inc.).

Conflict of Interest: The authors declare no competing financial interest.

Acknowledgment. This work was supported by Basic Science Research Program through the NRF funded by the Ministry of Education, Science, and Technology (2012R1A1A4A01008299, NO2012R1A1A2005772).

Supporting Information Available: Detailed consideration of quantum tunneling through MoS_2 barriers, nonlinearity of the carrier concentration with screening effect, current characteristics for doped MoS_2, calculation of density of states of AGNRs, and consideration of trigonal warping in graphene. This material is available free of charge *via* the Internet at http://pubs.acs.org.

REFERENCES AND NOTES

1. Novoselov, K. S.; Geim, A. K.; Morozov, S. V.; Jiang, D.; Katsnelson, M. I.; Griorieva, I. V.; Dubonos, S. V.; Firsov, A. A. Two-Dimensional Gas of Massless Dirac Fermions in Graphene. *Nature* **2005**, *438*, 197–200.
2. Zhang, Y.; Tan, Y.-W.; Stormer, H. L.; Kim, P. Experimental Observation of the Quantum Hall Effect and Berry's Phase in Graphene. *Nature* **2005**, *438*, 201–204.
3. Ghosh, S.; Bao, W.; Nika, D. L.; Subrina, S.; Pokatilov, E. P.; Lau, C. N.; Baladin, A. A. Dimensional Crossover of Thermal Transport in Few-Layer Graphene. *Nat. Mater.* **2010**, *9*, 555–558.
4. Lee, C.; Wei, X. D.; Kysar, J. W.; Hone, J. Measurement of the Elastic Properties and Intrinsic Strength of Monolayer Graphene. *Science* **2008**, *321*, 385–388.
5. Wu, Y.; Lin, Y.; Bol, A. A.; Jenkins, K. A.; Xia, F.; Farmer, D. B.; Zhu, Y.; Avouris, P. High-Frequency, Scaled Graphene Transistors on Diamond-like Carbon. *Nature* **2011**, *472*, 74–78.
6. Liao, L.; Lin, Y. C.; Bao, M.; Rui, C.; Bai, J.; Liu, Y.; Qu, Y.; Wang, K. L.; Huang, Y.; Duan, X. High-Speed Graphene Transistors with a Self-Aligned Nanowire Gate. *Nature* **2010**, *467*, 305–308.
7. Han, S. J.; Jenkins, K. A.; Garcia, A. V.; Franklin, A. D.; Bol, A. A.; Haensch, W. High-Frequency Graphene Voltage Amplifier. *Nano Lett.* **2011**, *11*, 3690–3693.
8. Yang, H.; Heo, J.; Park, S.; Song, H. J.; Seo, D. H.; Byun, K. E.; Kim, P.; Yoo, I.; Chung, H. J.; Kin, K. Graphene Barrister, a Triode Device with a Gate-Controlled Schottky Barrier. *Science* **2012**, *336*, 1140–1143.
9. Sabio, J.; Seoanez, C.; Fraini, S.; Guinea, F.; Castro Neto, A. H.; Sols, F. Electrostatic Interactions between Graphene Layers and Their Environment. *Phys. Rev. B* **2008**, *77*, 195409.
10. Ahn, G.; Kim, H. R.; Ko, T. Y.; Choi, K.; Watanabe, K.; Taniguchi, T.; Hong, B. H.; Ruy, S. Optical Probing of the Electronic Interaction between Graphene and Hexagonal Boron Nitride. *ACS Nano* **2013**, *7*, 1533–1541.
11. Britnell, L.; Gorbachev, R. V.; Jalil, R.; Belle, B. D.; Schedin, F.; Mishchenko, A.; Georgiou, T.; Katsnelson, M. I.; Eaves, L.; Morovoz, S. V.; *et al.* Field-Effect Tunneling Transistor Based on Vertical Graphene Heterostructures. *Science* **2012**, *335*, 947–950.
12. Mehr, W.; Dabrowski, J.; Christoph Scheytt, J.; Lippert, G.; Xie, Y. H.; Lemme, M. C.; Osting, M.; Lupina, G. Vertical Graphene Base Transistor. *IEEE Electron Device Lett.* **2012**, *33*, 691–693.
13. Fiori, G.; Bruzzone, S.; Iannaccone, G. Very Large Current Modulation in Vertical Heterostructure Graphene/hBN Transistor. *IEEE Trans. Electron Devices* **2013**, *60*, 268–273.
14. Bala Kumar, S.; Seol, G.; Guo, J. Modeling of a Vertical Tunneling Graphene Heterojunction Field-Effect Transistor. *Appl. Phys. Lett.* **2012**, *101*, 033503.
15. Butler, S. Z.; Hollen, S. M.; Cao, L.; Cui, Y.; Gupta, J. A.; Gutiérrez, H. R.; Heinz, T. F.; Hong, S. S.; Huang, J.; Ismach, A. F.; *et al.* Progress, Challenges, and Opportunities in Two-Dimensional Materials beyond Graphene. *ACS Nano* **2013**, *7*, 2898–2926.
16. Dean, C. R.; Young, A. F.; Meric, I.; Lee, C.; Wang, L.; Sorgenfrei, S.; Watanabe, K.; Taniguchi, T.; Kim, P.; Shepard, K. L.; *et al.* Boron Nitride Substrates for High-Quality Graphene Electronics. *Nat. Nanotechnol.* **2010**, *5*, 722–726.
17. Giovannetti, G.; Khomyakov, P. A.; Brocks, G.; Kelly, P. J.; Brink, J. V. Substrate-Induced Band Gap in Graphene on Hexagonal Boron Nitride: *Ab Initio* Density Functional Calculations. *Phys. Rev. B* **2007**, *76*, 073103.
18. Mayorov, A. S.; Gorbachev, R. V.; Morozov, S. V.; Britnell, L.; Jalil, R.; Ponomarenko, L. A.; Blake, P.; Novoselov, K. S.; Watanabe, K.; Taniguchi, T.; *et al.* Micrometer-Scale Ballistic Transport in Encapsulated Graphene at Room Temperature. *Nano Lett.* **2011**, *11*, 2396–2399.
19. Kim, S. M.; Hsu, A.; Araujo, P. T.; Lee, Y. H.; Palacios, T.; Dresselhaus, M.; Idrobo, J. C.; Kim, K. K.; Kong, J. Synthesis of Patched or Stacked Graphene and hBN Flakes: A Route to Hybrid Structure Discovery. *Nano Lett.* **2013**, *13*, 933–941.
20. Zhao, J.; Yu, Y.; Bai, Y.; Lu, B.; Wang, B. Chemical Functionalization of BN Graphene with the Metal-Arene Group: A Theoretical Study. *J. Mater. Chem.* **2012**, *22*, 9343–9350.
21. Li, Y.; Zhou, Z.; Zhang, S.; Chen, Z. MoS_2 Nanoribbons: High Stability and Unusual Electronic and Magnetic Properties. *J. Am. Chem. Soc.* **2008**, *130*, 16739–16744.
22. Ataca, C.; Şahin, H.; Aktürk, E.; Ciraci, S. Mechanical and Electronic Properties of MoS_2 Nanoribbons and Their Defects. *Phys. Chem. C* **2011**, *115*, 3934–3941.
23. Wang, Z.; Li, H.; Liu, Z.; Shi, Z.; Lu, J.; Suenaga, K.; Joung, S. K.; Okazaki, T.; Gu, Z.; Zhou, J.; *et al.* Mixed Low-Dimensional Nanomaterial: 2D Ultranarrow MoS_2 Inorganic Nanoribbons Encapsulated in Quasi-1D Carbon Nanotubes. *J. Am. Chem. Soc.* **2010**, *132*, 13840–13847.
24. Botello-Méndez, A. R.; Lópes-Urías, F.; Terrones, M.; Terrones, H. Metallic and Ferromagnetic Edges in Molybdebum Disulfide Nanoribbons. *Nanotechnology* **2009**, *20*, 325703.
25. Shidpour, R.; Manteghian, M. A Density Functional Study of Strong Local Magnetism Creation on MoS_2 Nanoribbon by Sulfur Vacancy. *Nanoscale* **2010**, *2*, 1429–1435.
26. Tongay, S.; Varnoosfaderani, S. S.; Appleton, B. R.; Wu, J.; Hebard, A. F. Magnetic Properties of MoS_2: Existence of Ferromagnetism. *Appl. Phys. Lett.* **2012**, *101*, 123105.
27. Kadantsev, E. S.; Hawrylak, P. Electronic Structure of a Single MoS_2 Monolayer. *Solid State Commun.* **2012**, *152*, 909–913.
28. Mak, K. F.; Lee, C.; Hone, J.; Shan, J.; Heinz, T. F. Atomically Thin MoS_2: A New Direct Band-Gap Semiconductor. *Phys. Rev. Lett.* **2010**, *105*, 136805.
29. Sundaram, R. S.; Engel, M.; Lombardo, A.; Krupke, R.; Ferrari, A. C.; Avouris, Ph.; Steiner, M. Electroluminescence in Single Layer MoS_2. *Nano Lett.* **2013**, *13*, 1416–1421.
30. Wu, S.; Huang, C.; Aivazian, G.; Ross, J. S.; Cobden, D. H.; Xu, X. Vapor-Solid Growth of High Optical Quality MoS_2 Monolayers with Near-Unity Valley Polarization. *ACS Nano* **2013**, *7*, 2768–2772.
31. Zhu, Z. Y.; Cheng, Y. C.; Schwingenschlögl, U. Giant Spin-Orbit-Induced Spin Splitting in Two-Dimensional Transition-Metal Dichalcogenide Semiconductors. *Phys. Rev. B* **2011**, *84*, 153402.
32. Sui, Y.; Appenzeller, J. Screening and Interlayer Coupling in Multilayer Graphene Field-Effect Transistor. *Nano Lett* **2009**, *9*, 2973–2977.

33. Ma, Y.; Dai, Y.; Guo, M.; Niu, C.; Huang, B. Graphene Adhesion on MoS_2 Monolayer: An *Ab Initio* Study. *Nanoscale* **2011**, *3*, 3883–3887.
34. Cao, T.; Wang, G.; Han, W.; Ye, H.; Zhu, C.; Shi, J.; Niu, Q.; Tan, P.; Wang, E.; Liu, B.; *et al*. Valley-Selective Circular Dichroism of Monolayer Molybdenum Disulphide. *Nat. Commun.* **2012**, *3*, 887.
35. Pereira, J. M., Jr.; Peeters, F. M.; Costa Filho, R. N.; Farias, G. A. Valley Polarization Due to Trigonal Warping on Tunneling Electrons in Graphene. *J. Phys.: Condens. Matter* **2009**, *21*, 045301.
36. Garcia-Pomar, J. L.; Cortijo, A.; Nieto-Vesperinas, M. Fully Valley-Polarized Electron Beams in Graphene. *Phys. Rev. Lett.* **2008**, *100*, 236801.
37. Aharony, A.; Tokura, Y.; Cohen, G. Z.; Entin-Wohlman, O.; Katsumoto, S. Filtering and Analyzing Mobile Qubit Information *via* Rashba-Dressenhaus-Aharonov-Bohm Interferometers. *Phys. Rev. B* **2011**, *84*, 035323.